Low-energy symmetric coplanar and symmetric non-coplanar (e, 2e) studies from the 3a₁ state of H₂O

Kate L Nixon[1]**, Andrew James Murray**[1]**, Ola Al-Hagan**[2]**, Don H Madison**[2] **and Chuangang Ning**[3]

[1] School of Physics and Astronomy, Photon Science Institute, University of Manchester, Manchester M13 9 PL, UK
[2] Department of Physics, Missouri University of Science and Technology, Rolla, MO 65409 USA
[3] Department of Physics and Key Laboratory of Atomic and Molecular NanoSciences of MOE, Tsinghua University, Beijing 100084, People's Republic of China

E-mail: Kate.Nixon-2@manchester.ac.uk

Abstract
Experimental and theoretical results are presented for electron impact ionization of water in the energy regime from near threshold to intermediate energies. Results were taken in symmetric coplanar and non-coplanar geometries, with both equal and non-equal outgoing electron energies. The models approximate the random orientation of the target using a spherical averaging of the wavefunction prior to the collision, using sophisticated distorted wave Born calculations that include post-collisional interactions in first order and to all orders of perturbation theory. The calculations predict the data most accurately at the lowest energy studied (4 eV above threshold) in a coplanar symmetric geometry, whereas the comparison between theory and experiment is generally marginal for higher energies and for non-coplanar geometries.

1. Introduction

Water is one of the most abundant molecules on earth. It is a relatively simple molecule and has attracted much attention over the years. The human body, and other biological material comprise ∼80% water, which makes water an ideal test case to investigate processes occurring in the body. As an example, energy deposition and angular distributions resulting from electron collisions with water are used in charged particle track structure analyses to model radiation damage in biological samples [1]. These models are an active area of research since the observation that high-energy radiation that is used to treat cancers also liberates many low-energy electrons, causing additional damage to cell DNA [2]. These low-energy electrons have an effect over a much wider volume than the targeted cancer site. Knowledge of the collision dynamics of low-energy electrons with biological systems is hence needed, so as to develop robust models of these processes. As a starting point, these biological systems are approximated as H_2O molecules.

(e, 2e) studies can be used to fully characterize the collision dynamics of electron impact ionization. In such experiments the energy and momenta of the outgoing electrons are measured, giving a fivefold-differential cross section. Despite this, only two experimental studies of electron impact ionization of H_2O at energies where the collision dynamics are important have been reported. The first used incident energies of ∼250 eV in an asymmetric coplanar configuration [3]. The second concentrated on the highest occupied molecular orbital (HOMO) at lower energies, i.e. <100 eV [4]. Consequently, only a limited number of theoretical investigations have been reported for incident energies below 300 eV [5]. Alternatively, (e, 2e) studies of H_2O at higher energies conducted under electron momentum spectroscopy conditions have been used to study the electronic structure of this chemically important molecule [6, 7], and these structure results are used to inform the models for lower energy collisions.

At incident energies less than ∼200 eV, the collision dynamics are strongly influenced by effects including post-collision interactions, target polarization, distortions in the

wavefunctions for the participating electrons and multiple collisions. In this regime these processes must be considered on an equal basis, and so the complexity of the interactions means that theoretical studies have mainly been limited to atomic targets. Current models are now at the stage where they yield reasonable agreement with experimental data for a range of atoms, implying a good understanding of the collision dynamics under the conditions used in the experiments, and these models are now being extended to low-energy (e, 2e) collisions from molecules.

Molecular targets provide a significant challenge to theory due to their distributed nuclei. This contrasts to atoms which have a single nuclear scattering centre, and which can hence be described using a spherical basis. Molecular wavefunctions are generally not spherical, the nuclei within the molecule providing multiple scattering centres. A key challenge in modelling electron collisions with molecules is hence in developing an accurate multi-centred wavefunction. A further challenge arises since the experiments cannot, at present, align the molecules prior to the collision; therefore, the models must consider the random orientation of the targets for accurate comparison with experiment. This becomes a computationally intensive problem, and so approximations are usually made to allow these calculations to become tractable.

Recently, experiments studying simple diatomic targets including H_2 and N_2 [8–12] have provided benchmark data to assess the performance of the new models that are being developed. The majority of data were recorded in a coplanar geometry, where the incident and two outgoing electrons are all in the same plane, and were conducted at a higher incident energy than the studies presented here. By contrast the apparatus at Manchester can also access *non-coplanar* geometries, and so has provided additional data to further test these models. Studies on more complex molecules at low energies are more limited, with only two measurements for CO_2 being reported [13, 14]. In this case no theoretical data were available for comparison with experiment.

H_2O has five molecular orbitals: $1a_1$, $2a_1$, $1b_2$, $3a_1$ and $1b_1$ (HOMO). The symmetry of the $2p_y$ oxygen atomic orbital, representing the lone pair of electrons on the oxygen atoms, prevents it from hybridizing with the H atomic orbital, leaving the molecular $1b_1$ HOMO orbital essentially atomic like, and therefore symmetric. In a previous study the groups at Manchester and Missouri investigated the $1b_1$ (HOMO) state of H_2O in coplanar kinematics [4]. However, the orientation averaged molecular orbital used in the theoretical calculation is not a good approximation for that state given the cancellations due to the orbital symmetry. By contrast, the $3a_1$ orbital of interest in this paper is involved in the O–H bonding and has a charge density distribution that is distorted from that of a symmetric atomic-like orbital. The molecular orbital used in the model therefore should not suffer from the same cancellation problem during the orientational averaging procedure. Thus, a comparison here between the theoretical predictions and the experimentally measured results should provide a much better assessment of the current models of the collision dynamics.

The remainder of this paper is presented in four sections. A brief description of the apparatus used to measure the
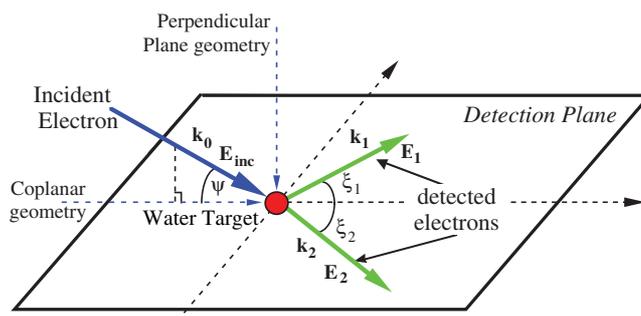

Figure 1. Schematic of the scattering geometry, depicting the various angles employed. A *coplanar geometry* ($\psi = 0°$) is defined when all three electrons are in the detection plane. The analyser angles (ξ_1 and ξ_2) are measured with respect to the projection of the incident electron beam $\mathbf{k_0}$ onto this plane as shown. For non-coplanar geometries the electron gun is lifted out of the plane, and is defined by the angle ψ. $\psi = 90°$ is called the *perpendicular geometry*.

(This figure is in colour only in the electronic version)

differential cross sections is given in section 2, where experimental considerations necessary to obtain good quality data are highlighted. Section 3 outlines the techniques used to generate the theoretical predictions. Both experimental and theoretical data are presented and discussed in section 4. Section 4.1 shows symmetric coplanar data, 4.2 gives symmetric non-coplanar data and section 4.3 shows data collected in both coplanar and perpendicular symmetric geometries with unequal energy sharing. Finally, section 5 draws conclusions from this investigation, and outlines future directions.

2. Experimental apparatus

The experimental triple-differential cross sections (TDCS) presented in section 4 were measured in the (e, 2e) apparatus at the University of Manchester. This apparatus is fully computer controlled and computer optimized, allowing it to operate continuously without user intervention. Full details of this spectrometer have been given previously [15–17] and so only a brief description is given here, with details pertinent to this study. The spectrometer can be operated in a 'standard' coplanar geometry where the momenta of all three electrons (the incident and two outgoing electrons) are within the same detection plane ($\psi = 0°$, figure 1). The electron gun can also rotate out of the detection plane, ($0° < \psi < 90°$) to access non-coplanar geometries, with $\psi = 90°$ being termed the *perpendicular geometry*. The two outgoing electron analysers rotate independently in the detection plane as shown. The analyser angles, ξ_1 and ξ_2, are referenced to the incident electron beam direction. In this study the analysers were always kept in a symmetric configuration, i.e. $\xi_1 = \xi_2 = \xi$.

The power supplies for the electrostatic lenses in the electron gun and the electron analysers are fully computer controlled and computer optimized. This feature allows for automated tuning of the spectrometer optics at regular intervals, with the analysers being re-optimized each time they
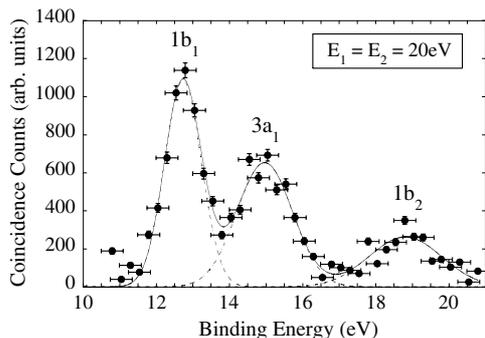
Figure 2. A typical coincidence binding energy spectrum obtained for H_2O. These data were measured in a coplanar geometry with outgoing electron energies of 20 eV detected at $\xi_1 = \xi_2 = 55°$. The peaks in the spectrum correspond to the three highest orbitals, i.e. the $1b_1$, $3a_1$ and $1b_2$ orbitals as labeled. The full line represents a three-Gaussian fit, whereas the dotted lines show the individual Gaussians from this fit, illustrating the degree of separation measured with the current energy resolution. Very little contamination is expected from neighbouring orbitals in the measured TDCS for the $3a_1$ state.

move to a new angle ξ. The energy of the spectrometer was re-calibrated at the start of each new kinematic arrangement, by measuring the coincidence binding energy spectrum. Here, the coincidence count rates as a function of incident energy are measured by scanning the incident electron beam energy (see figure 2). The coincidence energy resolution obtained with this apparatus was typically ~1.3 eV, which is sufficient to resolve the H_2O $3a_1$ orbital from those at higher and lower binding energies, as shown in figure 2. Over the course of this study the binding energy spectra were recorded for various energies and geometries, and it is estimated that contamination from neighbouring orbitals was always less than 10%, and is more typically in the range of 0.5%. The angular resolution of the apparatus is estimated as $\pm3°$, based on geometric considerations of the electrostatic lenses at those energies.

The distilled water sample used to provide the molecular target beam was contained within a 50 mm diameter 100 mm long stainless steel vessel sealed by a CF-70 flange to a 6.35 mm swagelok fitting. The vessel was connected to the scattering chamber via 6.35 mm copper tubing. A needle valve at the entrance to the scattering chamber controlled the flow of target H_2O vapour into the interaction region. The sample vessel and gas handling line were held at a constant temperature of 50 °C throughout data collection, so as to create sufficient driving pressure for the target beam. Several freeze-pump-thaw cycles were performed using a salted ice slurry bath, to remove dissolved gas impurities from the water prior to admission into the scattering chamber. The purity of the target beam was verified with a Spectra VacScan mass spectrometer fitted to the scattering chamber. Typical operational ratios of H_2O to N_2 were >25:1, and it was observed that the partial pressure of N_2 did not change appreciably from the background value when the needle valve was opened. This indicates that an H_2O target molecular beam of high purity was created, as confirmed from binding energy spectral studies. The purity of this beam was monitored regularly using the mass

spectrometer throughout this study. The background pressure within the scattering chamber was set to 1.1×10^{-5} torr during operation, and was found to remain constant throughout all data runs, in contrast to the observations of Milne-Brownlie *et al* [3] during their studies.

During these experiments we observed an unusual behaviour of the tungsten hairpin filament used as the incident electron source. Over time the emission current from the filament dramatically increased, when a constant current was delivered to the filament. This increase in emission current was often more than a factor of 2 within a 24 h period. To ensure constant incident electron beam current throughout the measurements as required, the filament current was hence also placed under computer control. To facilitate this, the current measured by the Faraday cup located on the opposite side of the interaction region to the electron gun was monitored by the computer control software, and the current through the filament adjusted to maintain a beam current of 300 nA throughout data collection. To illustrate the scale of these changes, over the duration of this work (~5 months) the filament current required to produce a beam current of 300 nA reduced from 2.1 A at commencement of these studies to less than 1.0 A. Previous measurements in this spectrometer also observed this effect [4], but did not find any explanation. In the present study we also measured the coincidence energy resolution from ionization of helium, and found that this did not change, indicating that the temperature of emission remained approximately constant. The reason for the steadily decreasing filament current is hence unknown at this time.

The first set of data presented in section 4.1 employ coplanar kinematics where the outgoing electron energies and polar angles of both analysers are the same, i.e. $E_1 = E_2$ and $\xi_1 = \xi_2$. Differential cross-section (TDCS) measurements using incident energies of 4 eV, 10 eV, 20 eV and 40 eV above the ionization potential of the $3a_1$ state (IP ~15 eV) over an angular range of 35–125° are presented in figure 3, along with the corresponding theoretical predictions. Section 4.2, and figure 4, shows data taken for symmetric kinematics where both outgoing electron energies are 10 eV. For these data sets the angle of the electron gun is varied from the standard coplanar geometry ($\psi = 0°$), through to $\psi = 90°$ for the perpendicular geometry. Finally, unequal energy sharing kinematics were investigated (figure 5) as discussed in section 4.3. Here, the angles of the analysers were equal, $\xi_1 = \xi_2$; the incident electron energy was 20 eV above the ionization threshold and the energies of the outgoing electrons were set to be *unequal*. The first set of data used $E_1 = 18$ eV and $E_2 = 2$ eV, while the second used $E_1 = 15$ eV and $E_2 = 5$ eV. Data were measured only for coplanar and perpendicular geometries, over angular ranges from 22.5° to 130° and 35° to 140° respectively.

All data presented here were taken using a constant chamber pressure and constant beam current as noted above. The data were normalized to a collection time of 1000 s for each measurement, and up to 30 angular sweeps of the detection plane were used to produce statistically significant results. The data presented in figures 3–5 were then averaged over these sweeps, and the uncertainties in the measurements
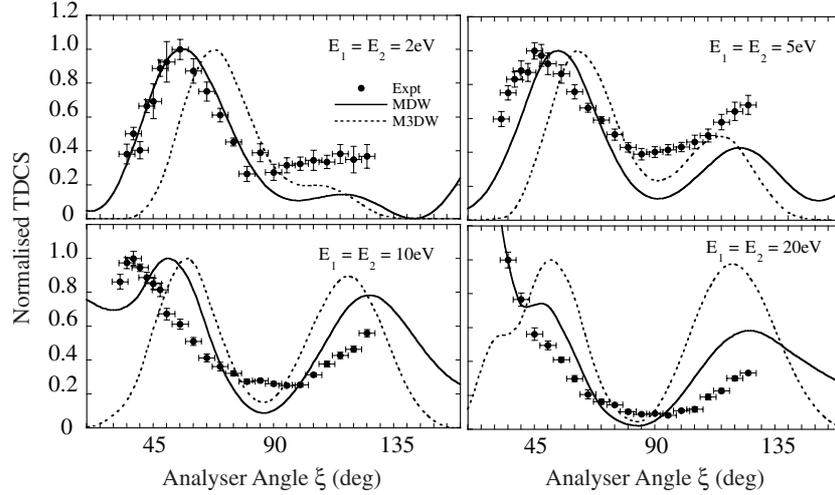
Figure 3. Triple-differential cross sections for ionization of the $3a_1$ state of H_2O using coplanar symmetric kinematics (i.e. $\psi = 0°$ and $\xi_1 = \xi_2$). The energies of the outgoing electrons are shown on the respective plots. The solid line shows results from the molecular distorted wave Born approximation (MDW) while the dashed line was generated from the molecular 3-body distorted wave approximation (M3DW). The experimental and theoretical data have been independently normalized to unity at each energy.
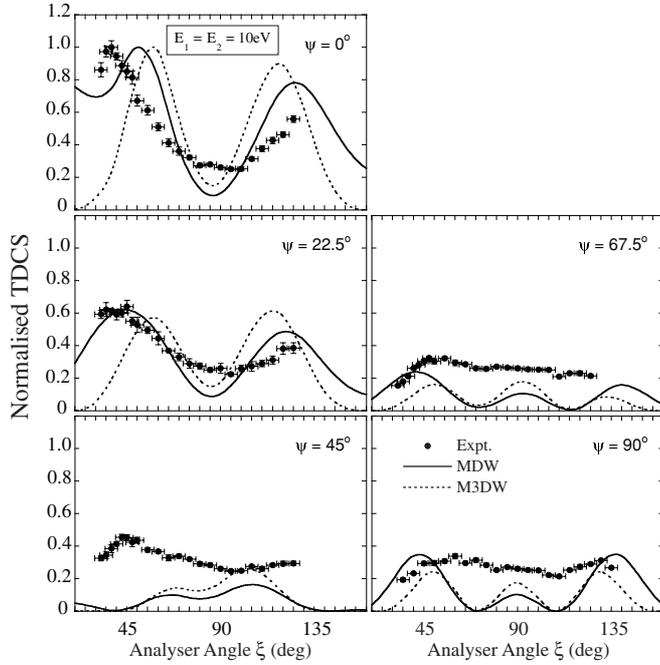

Figure 4. Triple-differential cross sections for the ionization of the $3a_1$ state of H_2O. These measurements were taken in a series of symmetric non-coplanar geometries with outgoing electron energies of 10 eV. The angle of the electron gun (ψ) is shown on the respective plots. The data and theory are normalized to unity at the peak in the coplanar ($\psi = 0°$) geometry. The data within the remaining plots are normalized at the $\xi = 90°$ point (see the text for details).

determined from the complete set of data for each scattering angle.

3. Theoretical framework

The molecular 3-body distorted wave (M3DW) approximation has been presented in previous publications [18–20] so only a

brief outline of the theory will be given. The triple-differential cross section (TDCS) for the M3DW is given by

$$\frac{d^5\sigma}{d\Omega_a \Omega_b\, dE_b} = \frac{2}{(2\pi)^5}\frac{k_a k_b}{k_i}|T|^2 \qquad (1)$$

where $\vec{k}_i$, $\vec{k}_a$ and $\vec{k}_b$ are the wave vectors for the initial, scattered and ejected electrons, respectively. The amplitude is given by

$$T = \langle \chi_a^-(\vec{k}_a, \mathbf{r}_1)\chi_b^-(\vec{k}_b, \mathbf{r}_2)C_{\text{scat-eject}}(\mathbf{r}_{12}^{\text{ave}})$$
$$\times |V - U_i|\phi_j^{OA}(\mathbf{r}_2)\chi_i^+(\vec{k}_i, \mathbf{r}_1)\rangle \qquad (2)$$

where r_1 and r_2 are the coordinates of the incident and the bound electrons, χ_i, χ_a and χ_b are the distorted waves for the incident, scattered and ejected electrons respectively, and $\phi_j^{OA}(\mathbf{r}_2)$ is the initial bound-state wavefunction which is approximated as the orientation averaged molecular wavefunction for the molecular orbital of interest. The molecular wavefunction was calculated using density functional theory (DFT) along with the standard hybrid B3LYP [21] functional by means of the ADF 2007 (Amsterdam Density Functional) program [22] with the TZ2P (triple-zeta with two polarization functions) Slater-type basis sets. The factor $C_{\text{scat-eject}}(r_{12}^{\text{ave}})$ is the Ward–Macek average Coulomb-distortion factor between the two final-state electrons [23], V is the initial state interaction potential between the incident electron and the neutral molecule and U_i is a spherically symmetric distorting potential which is used to calculate the initial-state distorted wave for the incident electron $\chi_i^+(\vec{k}_i, \mathbf{r}_1)$.

The Schrödinger equation for the incoming electron wavefunction is given by

$$\left(T + U_i - \frac{k_i^2}{2}\right)\chi_i^+(\vec{k}_i, \mathbf{r}_1) = 0 \qquad (3)$$

where T is the kinetic energy operator and the '+' superscript on $\chi_i^+(\vec{k}_i, \mathbf{r}_1)$ indicates outgoing wave boundary conditions. The initial state distorting potential contains three components $U_i = U_s + U_E + U_{CP}$, where U_s is the
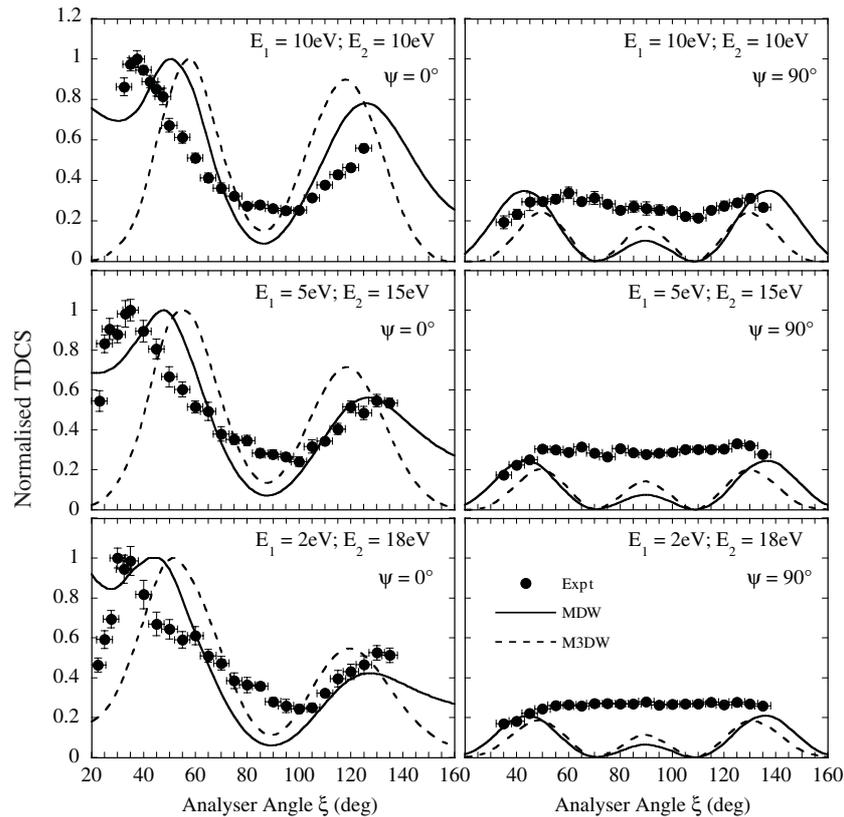
Figure 5. Triple-differential cross sections for ionization of the $3a_1$ state of H_2O. Symmetric geometries were adopted for these data with unequal energy sharing kinematics. Both coplanar and perpendicular geometries were utilized. In all plots the excess energy is 20 eV, with the outgoing electron energies as shown. The electron gun angle ψ is also shown in the respective plots.

initial state spherically symmetric static potential which is obtained from the molecular charge density averaged over all angular orientations, U_E is the exchange potential of Furness–McCarthy (corrected for sign errors) [24] which approximates the effect of the continuum electron exchanging with the passive bound electrons in the molecule and U_{CP} is the correlation–polarization potential of Perdew and Zunger [25, 26].

The final state for the system is approximated as a product of distorted waves for the two continuum electrons times the average Coulomb-distortion factor. The final state distorted waves are calculated as for the initial state except that the final state spherically symmetric static distorting potential for the molecular ion is used for U_s.

The molecular distorted wave Born approximation (MDW) is the same calculation as the M3DW except that the post-collision-interaction (PCI) factor $C_{\text{scat-eject}}\left(r_{12}^{\text{ave}}\right)$ is not included in the calculations.

4. Results and discussion

4.1. Symmetric coplanar kinematics

The experimental data recorded here are not measured on an absolute scale and so to compare experiment and theory both are normalized to a maximum intensity of unity at each energy, as shown in figure 3. The experimental data show the typical characteristics expected from measurements such

as these. There is a strong peak at forward scattering angles ($\xi < 90°$) and a peak at backward scattering angles ($\xi > 90°$). The overall shape of the TDCS measured at corresponding energies in a previous study of the $1b_1$ state [4] are qualitatively similar; however, the $1b_1$ state shows a second peak in the forward region emerging at higher energies that is not observed in the $3a_1$ state measured here. Milne-Brownlie *et al* [3] also noted that these two outer-most orbitals have a similar structure using different kinematical conditions to those used here.

As the energy of the outgoing electrons is lowered, it would be expected that the Coulomb repulsion between the outgoing electrons should play an increasingly important role, driving the electrons apart. This repulsion is normally called the post-collision interaction (PCI). PCI would cause the forward peak to shift towards $\xi = 90°$ as is seen in the data. PCI would also be expected to shift the backward peak towards $\xi = 90°$, although this cannot be confirmed in the data as the peak is beyond the angular range measured in this experiment. This trend is much clearer in the present data compared to that from the $1b_1$ state measured at higher energies [4]. The only difference between the two theoretical calculations shown in the figure is that M3DW contains PCI to all orders of perturbation theory while MDW only has PCI to first order, and it is clearly seen that PCI shifts the forward and backward peaks towards $\xi = 90°$ as would be expected. However, it appears that PCI is too strongly represented in the M3DW since the peak positions of the MDW are closer to the experimental data.

Interestingly, the best agreement between experimental data and theory is at the lowest energy, where the experimental data and MDW model are in excellent agreement for the forward peak. This agreement diminishes as the energy increases, which is unexpected since the MDW model is usually more accurate at higher energies.

4.2. Symmetric non-coplanar kinematics

A key advantage of the spectrometer in Manchester is the ability to measure data for kinematics in non-coplanar geometries. Non-coplanar measurements were hence taken here with both outgoing electrons having an energy of 10 eV. As seen in figure 1, the geometry adopted in this spectrometer provides a common normalization point ($\xi_1 = \xi_2 = 90°$) for all gun angles ψ, which allows ALL data at a given energy to be referenced to a common point. For the current measurements, the data at $\psi = 0°$ have been normalized to a maximum intensity of unity, as before. The value of the TDCS at $\xi = 90°$ is then used to re-normalize the remaining data. For the corresponding theoretical model, the coplanar TDCS has also been normalized to unity for both MDW and M3DW models. This scaling factor is then applied to all subsequent data sets at the various gun angles.

The experimental data in figure 4 show a clear trend indicating that the forward and backward peaks diminish in magnitude as the angle of the electron gun increases from $\psi = 0°$ to $90°$. The TDCS measured in the perpendicular plane is almost constant over all angles ξ, which is very different to what is observed for atomic targets. The data contrast strongly with the theoretical predictions for the larger gun angles ψ, where the theories predict significantly more structure than is seen in the data. The progression in both models shows a decrease in cross section from $\psi = 0°$ to $45°$, after which the intensity once again increases. Neither model accurately predicts the results that have been obtained experimentally.

The results found here are in strong contrast to what we have found earlier for H_2 [27]. For that case, excellent agreement between theory and experiment was found for the perpendicular plane and the agreement was not nearly as satisfactory in the scattering plane ($\psi = 0°$), yet here we find better agreement in this plane than the perpendicular plane. Also Al-Hagan *et al* [27] predicted that molecules which have nuclei at the centre of mass should have a TDCS with three peaks at $45°$, $90°$ and $135°$ in the perpendicular plane. The $45°$ and $135°$ peaks would be a result of elastic scattering of the projectile with the target bringing the projectile into the perpendicular plane followed by a binary electron–electron collision. The $90°$ peak should result from elastic scattering of the projectile with the target bringing the projectile into the perpendicular plane, followed by binary electron–electron collision, and finally a $180°$ backscattering of one of the electrons from the nuclei at the centre of mass. While this prediction was verified for CO_2, here for H_2O theory is consistent with the prediction while experiment shows almost no structure at all for the perpendicular plane.

4.3. Unequal energy sharing, coplanar and perpendicular geometries

The final kinematic configuration investigated here used symmetric geometries and 20 eV excess energy as above; however, in this case the data are for *unequal* energy sharing between the outgoing electrons. The data were only taken for coplanar ($\psi = 0°$) and perpendicular plane ($\psi = 90°$) geometries, so as to contrast differences in these two extremes. Figures 5(a) and (b) reproduce the data in figure 3 at these angles when $E_1 = 10$ eV and $E_2 = 10$ eV, figures 5(c) and (d) show data for $E_1 = 5$ eV and $E_2 = 15$ eV, while figures 5(e) and (f) show results for $E_1 = 2$ eV and $E_2 = 18$ eV. The theoretical calculations using the M3DW and MDW models are also shown, where once again the data and theory have been normalized to unity at the peak in the coplanar geometry.

The key differences that can be seen in these data for the coplanar geometry are that the forward peak moves to a smaller angle as the energy asymmetry increases, as might be expected from post-collisional interactions. Again for the backward peak, there is not enough data to see this effect at high angles. There also appears to be a narrowing in the main forward peak as the asymmetry increases, with a new shoulder appearing around $\xi = 60°$. The minimum around $90°$ in this geometry does not change substantially as the energy sharing changes.

The M3DW and MDW calculations in the coplanar geometry predict the relative magnitudes of the forward and backward peaks for the highest asymmetry, but again the MDW is in better agreement with the experimental peak positions, which is surprising. The position of the minimum is predicted well in all cases, however not the relative magnitude.

In the perpendicular plane the experimental cross section becomes almost completely featureless at the highest asymmetry, although none of the data show any significant structure. This contrasts markedly with the calculations, which predict clear triple peaks in the perpendicular plane that change magnitude only marginally with the asymmetry. The magnitude of the data for equal energy sharing is approximated by the calculation, but this agreement is less satisfactory as the asymmetry increases.

5. Conclusions

Experimental (e, 2e) data for the ionization of water at low energies in both coplanar and non-coplanar geometries have been compared with state of the art theoretical results derived from distorted wave models. The theory models the molecules in a spherically averaged basis to allow for the random orientation of the target in the experiments, and considers the effects of post-collisional interactions.

Agreement between theory and experiment is mixed, and rather surprisingly gives best results at low energies, where it might be expected that the approximations are least accurate. The results using the full M3DW model (which includes PCI to all orders) appear to overestimate the effects of PCI compared to the MDW theory which only includes PCI to first order.

This is particularly seen for coplanar symmetric data 4 eV above threshold, where the forward peak is reproduced more accurately using the MDW calculation.

For non-coplanar measurements the comparison between theory and experiment becomes poorer as the gun angle increases, in contrast to previous results from H_2 which show the opposite trend. This discrepancy is seen both for equal energy and for non-equal energy data, which have been taken in coplanar and perpendicular geometries. The experimental results for both equal and non-equal energy sharing in the perpendicular plane show almost no structure, whereas the theoretical calculations predict that three clearly defined lobes should be seen.

It is clear from these results that significant discrepancies remain between the models and the experimental data for this important target. These differences may be arising from the approximations made in calculating the spherically averaged wavefunction input to the model, as are used to emulate the random orientation of the targets in the experiment. The results clearly highlight the need for both experiment and theory to provide more exacting data. From the experimental side, it is clearly important to orient the target prior to the collision occurring, whereas theory needs to perform more exacting calculations using a fixed molecular axis, before summing over all possible orientations of the targets so as to yield accurate comparison to experiment. We are considering techniques to try to solve these experimental difficulties, and are investigating the computational challenges that must be overcome to provide more exact theoretical results. It is hoped that in the near future improvements will be forthcoming in both areas, so that robust models of these more complex molecular targets can be derived.

Acknowledgments

References

[1] Munoz A, Blanco F, Garcia G, Thorn P A, Brunger M J, Sullivan J P and Buckman S J 2008 *Int. J. Mass Spectrom.* **277** 175
[2] Boudaiffa B, Cloutier P, Hunting D, Huels M A and Sanche L 2000 *Science* **287** 1658
[3] Milne-Brownlie D S, Cavanagh S J, Lohmann B, Champion C, Hervieux P A and Hanssen J 2004 *Phys. Rev.* A **69** 032701
[4] Kaiser C, Spieker D, Gao J F, Hussey M, Murray A and Madison D H 2007 *J. Phys.* B **40** 2563
[5] Champion C, Hanssen J and Hervieux P A 2002 *Phys. Rev.* A **65** 022710
[6] Bawagan A O, Brion C E, Davidson E R and Feller D 1987 *Chem. Phys.* **113** 19
[7] Dixon A J, Dey S, McCarthy I E, Weigold E and Williams G R J 1977 *Chem. Phys.* **21** 81
[8] Staicu Casagrande E M *et al* 2008 *J. Phys.* B **41** 025204
[9] Colgan J, Al-Hagan O, Madison D H, Kaiser C, Murray A J and Pindzola M S 2009 *Phys. Rev.* A **79** 052704
[10] Milne-Brownlie D S, Foster M, Gao J F, Lohmann B and Madison D H 2006 *Phys. Rev. Lett.* **96** 233201
[11] Murray A J, Hussey M J, Gao J F and Madison D H 2006 *J. Phys.* B **39** 3945
[12] Naja A, Staicu Casagrande E M, Lahham-Bennani A, Nekkab M, Mezdari F, Joulakian B, Chuluunbaatar O and Madison D H 2007 *J. Phys.* B **40** 3775
[13] Hussey M J and Murray A J 2005 *J. Phys.* B **38** 2965
[14] Lahmam-Bennani A, Staicu Casagrande E M and Naja A 2009 *J. Phys.* B **42** 235205
[15] Murray A J, Turton B C H and Read F H 1992 *Rev. Sci. Instrum.* **63** 3346
[16] Murray A J and Read F H 1993 *Phys. Rev.* A **47** 3724
[17] Murray A J and Cvejanovic D 2003 *J. Phys.* B **36** 4875
[18] Gao J F, Madison D H and Peacher J L 2005 *J. Chem. Phys.* **123** 204314
[19] Gao J F, Madison D H and Peacher J L 2005 *Phys. Rev.* A **72** 032721
[20] Gao J F, Peacher J L and Madison D H 2005 *J. Chem. Phys.* **123** 204302
[21] Lee C T, Yang W T and Parr R G 1988 *Phys. Rev.* B **37** 785
[22] Guerra C F, Snijders J G, te Velde G and Baerends E J 1998 *Theo. Chem. Acc.* **99** 391
[23] Ward S J and Macek J H 1994 *Phys. Rev.* A **49** 1049
[24] Furness J B and McCarthy I E 1973 *J. Phys.* B **6** 2280
[25] Perdew J P and Zunger A 1981 *Phys. Rev.* B **23** 5048
[26] Padial N T and Norcross D W 1984 *Phys. Rev.* A **29** 1742
[27] Al-Hagan O, Kaiser C, Madison D H and Murray A J 2009 *Nature Phys.* **5** 59